ELSEVIER

Journal of Neuroscience Methods 143 (2005) 179–195

JOURNAL OF NEUROSCIENCE METHODS

www.elsevier.com/locate/jneumeth

Methods for functional magnetic resonance imaging in normal and lesioned behaving monkeys

Mark A. Pinsk[a,b], Tirin Moore[c], Marlene C. Richter[b], Charles G. Gross[a], Sabine Kastner[a,b,*]

[a] *Department of Psychology, Princeton University, Green Hall, Princeton, NJ 08544, USA*
[b] *Center for the Study of Brain, Mind, and Behavior, Princeton University, Green Hall, Princeton, NJ 08544, USA*
[c] *Department of Neurobiology, Stanford University School of Medicine, Sherman, Fair child Building, Stanford, CA 94305, USA*

Received 23 July 2004; received in revised form 6 October 2004; accepted 6 October 2004

Abstract

Methods for performing functional magnetic resonance imaging (fMRI) studies in behaving and lesioned monkeys using a human MR scanner are reported. Materials for head implant surgery were selected based on tests for magnetic susceptibility. A primate chair with a rigid head fixation system and a mock scanner environment for training were developed. To perform controlled visual studies, monkeys were trained to maintain fixation for several minutes using a novel training technique that utilized continuous juice rewards. A surface coil was used to acquire anatomical and functional images in four monkeys, one with a partial lesion of striate cortex. High-resolution anatomical images were used after non-uniform intensity correction to create cortical surface reconstructions of both lesioned and normal hemispheres. Our methods were confirmed in two visual experiments, in which functional activations were obtained during both free viewing and fixation conditions. In one experiment, face-selective activity was found in the fundus and banks of the superior temporal sulcus and the middle temporal gyrus in monkeys viewing pictures of faces and objects while maintaining fixation. In a second experiment, regions in occipital, parietal, and frontal cortex were activated in lesioned and normal animals viewing a cartoon movie. Importantly, in the animal with the striate lesion, fMRI signals were obtained in the immediate vicinity of the lesion. Our results extend those previously reported by providing a detailed account of the technique and by demonstrating the feasibility of fMRI in monkeys with lesions.

Keywords: fMRI; Lesioned monkeys; BOLD; Face responses

1. Introduction

Functional magnetic resonance imaging (fMRI) has become an important tool for studying human brain function (e.g. Kastner and Ungerleider, 2000). More recently, this technique has been applied to the macaque monkey, which is the most widely studied animal model for human neocortical organization and function. For several reasons, the use of fMRI in monkeys is of considerable potential for understanding brain function, especially when applied in conjunction with invasive techniques. First, functional brain mapping techniques yield information about the organization of distributed neural processing at a large-scale population level, thereby complementing results from single- and multi-unit recording studies. Second, brain regions involved with perception, motor function and cognition can be easily localized to identify sites for traditional invasive experimental approaches such as single cell recordings or lesions. Third, the use of fMRI in animals with focal brain lesions provides a unique model to study recovery of brain function and behavior at the level of distributed large-scale networks. Fourth, in combination with microelectrode recordings, the application of fMRI in monkeys helps to clarify the relation between neural signals and the blood oxygenation dependent (BOLD) signal acquired with fMRI (Logothetis et al., 2001).

* Corresponding author. Tel.: +1 609 258 0479; fax: +1 609 258 1113.
E-mail address: skastner@princeton.edu (S. Kastner).

0165-0270/$ – see front matter © 2004 Elsevier B.V. All rights reserved.
doi:10.1016/j.jneumeth.2004.10.003

And fifth, fMRI studies in awake, behaving monkeys and in humans using similar experimental paradigms hold the promise of revealing similarities and differences in the organization of brain areas in the two species (Denys et al., 2004; Kourtzi et al., 2003; Koyama et al., 2004; Nakahara et al., 2002; Orban et al., 2003; Tsao et al., 2003a,b; Vanduffel et al., 2002).

Significant technical challenges must be overcome to perform fMRI studies in awake, behaving monkeys using a human MR scanner (Dubowitz et al., 1998; Stefanacci et al., 1998; Vanduffel et al., 2001). All devices, such as the apparatus for restraining the monkey's head and the reward apparatus, must be constructed from MR compatible materials that do not interfere with the signal acquisition. Further, due to the horizontal bore of most human MR scanners, the animals must be restrained in a horizontal position and need to be specifically trained to perform behavioral tasks in a noisy environment and extremely confined space. Here, we describe methods we have developed to perform fMRI studies in awake, behaving animals trained to fixate for extended periods of time. These include evaluating materials for head post implants, the design and construction of an MR compatible primate chair and a mock scanner setup, and the development of adequate training procedures. Our methods were then applied in two studies. In the first study, our goal was to establish functional brain imaging in behaving monkeys with circumscribed brain lesions. Visually-evoked functional activations obtained during free viewing of a cartoon movie were compared in monkeys with and without partial lesions of striate cortex to determine whether BOLD signals in the vicinity of the lesion could be measured. In the second study, our goal was to determine whether specific stimulus-related activity could be obtained in animals trained to fixate for several minutes. Activity in visual cortex related to presentations of faces, objects and scrambled pictures was studied in two of our trained animals.

Several previous studies have described methods to perform fMRI experiments in anesthetized and awake monkeys (Denys et al., 2004; Dubowitz et al., 1998, 2001; Koyama et al., 2004; Nakahara et al., 2002; Stefanacci et al., 1998; Tsao et al., 2003a,b; Vanduffel et al., 2001, 2002). Procedures for evoking activity related to sensory stimulation in visual and parietal cortex have been reported (Disbrow et al., 1999; Dubowitz et al., 1998; Leopold et al., 2002; Logothetis et al., 1999; Rainer et al., 2001, 2002; Sereno et al., 2002; Stefanacci et al., 1998; Tolias et al., 2001). Further, the use of contrast agents has been shown to enhance signal detection in both anesthetized and awake animals (Dubowitz et al., 2001; Vanduffel et al., 2001; Leite et al., 2002). Our study extends previous reports by providing a detailed account of training, scanning, and image processing procedures, and by demonstrating the feasibility of fMRI in animals with cortical lesions. Part of this work has been published in abstract form (Pinsk et al., 2003).

2. General materials and methods

Standard methods for surgical procedures, visual stimulation, experimental design, data acquisition and analysis are described in this section. Methods that were developed specifically for monkey fMRI are described in Section 3.

2.1. Subjects

Subjects were four adult, male macaque monkeys (*Macaca fascicularis*) weighing 4–9 kg. All procedures were approved by the Princeton University Animal Care and Use Committee and conformed to NIH guidelines for the humane care and use of laboratory animals.

2.2. Surgical procedures

All surgical procedures were performed under strictly aseptic conditions and under general anesthesia with isoflurane (induction 2–4%, maintenance 0.5–2%) following preanesthetic medication with atropine (0.08 mg/kg i.m.), ketamine (2–10 mg/kg i.m.) and acepromazine (1 mg/kg). In all animals, a plastic head bolt (Model CILUX FHP/D-J9; Crist Instrument Inc., Damascus, MD, USA) for restraining the head was implanted to extend vertically from the rostral cranium using ceramic screws ($ZrO_2 + Y_2O_3$; Ceramco Inc., Center Conway, NH, USA) and dental acrylic (Cross-Linked Flash Acrylic; Yates & Bird Co., Chicago, IL, USA). All materials used for implant surgery were tested for magnetic susceptibility prior to surgery (see Section 3 for details). The animals were treated post-surgically with antibiotics (e.g. Baytril, 2.5 mg/kg i.m.) and analgesics (e.g. Buprenorphine, 0.01 mg/kg i.m.). Wound margins of skin surrounding the implant were cleaned regularly. One animal received a partial unilateral ablation of striate cortex in a second surgery. Protocols for anesthesia and post-surgical treatments were as in the first surgery. Surgical methods were similar to those described in detail previously (Rodman et al., 1989; Moore et al., 1996; Moore et al., 2001). Briefly, lesion surgery was performed after removal of the overlying bone and turning a dural flap. Striate cortex on the lateral surface, the medial surface and in the calcarine fissure (representing the central 8–12° of the visual field) was removed by subpial aspiration under the control of a Zeiss operating microscope. The dural flap and the soft tissues around the edge of the wound were then sutured.

2.3. Visual stimulation and experimental design

In experiment 1, three normal animals (M1, M2, and M3) and one animal with a unilateral striate lesion (M4) viewed a cartoon movie. The movie was displayed from a DVD player and projected from an Epson LCD projector onto a translucent screen located at the back of the scanner bore at a distance of 60 cm from the animals' eyes and subtending $30^\circ \times 30^\circ$ of visual angle. The movie presentation was synchronized to

the beginning of each scan manually with a keyboard button press. Movie clips of 30 s were presented in alternation with periods of blank screens (i.e. no visual stimulation, mean luminance of 0.50 cd/m^2) of the same length. Three blocks of visual stimulation ($\sim$150 cd/m^2) were presented during a given run of 210 s, which started and ended with a 30-s blank period. Each run was repeated six times during a scanning session. Monkeys viewed the cartoon movie freely, and were given juice after each run. Eye positions were monitored during the scanning sessions using a long-range infrared eye tracking system (see Section 3 for details).

In experiment 2, two normal animals (M1, M2) were shown color pictures of objects, faces, and phase-scrambled pictures while maintaining fixation. The stimuli subtended $5^\circ \times 5^\circ$ and were presented for 1 s foveally behind the fixation point (0.50° diameter) followed by a 1 s blank interval during which only the fixation point was present. Blocks of stimuli from each category were presented interleaved with blank periods, each lasting 12 s. Each category block was repeated twice in a scan, resulting in scans of 192 s each. The stimulus presentation and eye position recording was synchronized to the beginning of each scan using a trigger pulse from the scanner. The monkey received a juice reward at regular intervals (1–2 s) when it maintained fixation within a square window of 4° of visual angle during the stimulus blocks and the blank periods (see Section 3.4 for more details). Scans during which the animal broke fixation for longer than 500 ms more than 20 times were excluded from analysis. The animal completed 8–10 scans in each session before becoming satiated with juice. We report data from four scanning sessions that were combined for a total of 3000 volumes.

2.4. Data acquisition and analysis

Structural and functional images were acquired with a 3 T head-dedicated scanner (Magnetom Allegra; Siemens, Erlangen, Germany) designed for human brain scanning, using a 12-cm transmit/receive surface coil (Model NMSC-023; Nova Medical Inc., Wakefield, MA, USA). Monkey subjects were placed in the 'sphinx' position in an MR-compatible primate chair during scanning sessions (see Section 3.2). In order to perform cortical surface reconstructions offline, a high resolution (0.5 mm × 0.5 mm × 0.5 mm) structural scan was acquired in a session lasting for 3 h and 33 min [i.e. the extra-session anatomical scan; MPRAGE sequence; FOV = 128 mm × 128 mm; 256 × 256 matrix; TR = 2500 ms; TE = 4.4 ms; TI = 1100 ms; flip angle = 8°; 20 acquisitions], during which the animals were anesthetized with Telazol (tiletamine/zolazepam, 10 mg/kg i.m.). All other scan sessions, each lasting about 2 h, were performed with awake animals. Functional images were taken with a gradient echo, echo planar sequence (FOV = 80 mm × 80 mm; 64 × 64 matrix; TR = 2000 ms, TE = 32 ms, flip angle = 90°, bandwidth = 2112 Hz/Pixel). Twenty-six contiguous coronal slices (thickness = 2 mm without gap, in-plane resolution: 1.25 mm × 1.25 mm) were acquired in 6 series of 105 images each (experiment 1) or 8–10 series of 130 images each (experiment 2), starting from the posterior pole and covering the brain up to the region of the principal sulcus. Prior to acquiring the functional scans, an automatic shim was performed over the posterior half of the brain to improve the signal-to-noise ratio and reduce susceptibility artifacts caused by the ear canals and head implant. A high-resolution anatomical scan lasting 11 min (i.e. the intra-session anatomical scan) was also acquired in the same session (0.5 mm × 0.5 mm × 1.0 mm, MPRAGE sequence; FOV = 128 mm × 128 mm; 256 × 256 matrix; TR = 2500 ms; TE = 4.4 ms; TI = 1100 ms; flip angle = 8°; 1 acquisition) for alignment with the extra-session anatomical scan from which the cortical surface was reconstructed.

The first four images in each functional scan were excluded from analysis to avoid using images acquired before magnetization equilibrium was reached. In experiment 1, the functional images were motion-corrected by registering each image to the image acquired closest in time to the high-resolution anatomical scan using a 3D registration tool provided by the AFNI software package (Version 2.55; Cox, 1996; Cox and Hyde, 1997). Despite being head-restrained, motion correction is necessary to correct for residual head motion that the head restraint may not prevent and for phase drift due to shim heating during the scanning session. The registration tool is designed to be efficient at correcting head motions of a few millimeters and head rotations of a few degrees. It uses an iterated linearized weighted least squares algorithm and Fourier interpolation to match each volume to the reference volume (Cox and Jesmanowicz, 1999). In experiment 2, the functional images from four sessions of monkey M2 and five sessions of monkey M1 were motion corrected to a single image acquired in the first session of each animal using the same registration tool. Because the animal's head position and the slice prescription were exactly replicated across scan sessions, we were able to register all of the images from all sessions to the same reference image. For both experiments, the images were spatially filtered with a small 2 mm Gaussian kernel to increase the signal-to-noise ratio but still retain spatial specificity. For experiment 2, in order to combine data from multiple sessions, the data were first normalized to their means using the following formula: $c = (a - b)/b \times 100$ where a is the motion-corrected and spatially filtered voxel intensity in a time series, b the mean intensity value of that voxel, and c is the normalized intensity value of that voxel. For both experiments, statistical analyses were performed using multiple regression in the framework of the general linear model (Friston et al., 1995) using the AFNI software package.

Square-wave functions matching the time course of the experimental design were defined as effects of interest in the multiple regression model. Each of the square-wave functions was convolved with a gamma-variate function to generate idealized response functions (Cohen, 1997), which were used as

regressors of interest in the multiple regression model. In addition, regressors that accounted for variance due to baseline shifts between time series, linear drifts within time series, and head motion parameter estimates calculated by the registration were included into the regression model. For experiment 1, we contrasted visual stimulation versus blank. For experiment 2, we contrasted objects versus scrambled pictures, faces versus scrambled pictures, and faces versus objects. Statistical maps for experiments 1 and 2 were thresholded at a z score of 3.72 ($p < 0.0001$). The statistically significant voxels were overlaid on the intra-session T1-weighted anatomical volume by using the volume position parameters obtained during the scan session.

In experiment 1, regions of interest (ROIs) were defined using sulcal landmarks on the T1-weighted anatomical volume. The raw fMRI signals were averaged across all activated voxels ($z > 3.72$, $p < 0.0001$) within a given ROI and across scans, and normalized to the mean intensity obtained during the blank periods.

Several steps were performed to project the activated voxels onto the reconstructed cortical surfaces. First, the intra-session anatomical volume was registered and resampled using cubic interpolation to the higher resolution extra-session volume using AFNI's 3D registration tool (Cox and Jesmanowicz, 1999), and visually checked for alignment accuracy. Second, the statistical maps were registered and resampled using a nearest neighbor interpolation method to the higher resolution extra-session volume using the rotation and translation parameters from the previous anatomical registration. With this interpolation method the value of a voxel at a specific location is given by the value of the original voxel that is closest to the new one, thus eliminating any interpolation of statistical values. Once the statistical maps were aligned to the extra-session volume, the significantly activated voxels could be projected onto the cortical surface reconstructions for visualization purposes.

3. Results and discussion

3.1. Materials for head post implants

Each monkey received a head bolt implant to restrain the animal's head in a fixed position in the primate chair and to minimize head motion. When different materials are placed in close proximity to one another in an MR-environment, they have the potential to cause image artifacts due to their differing magnetic susceptibilities (Buxton, 2001). Because only materials that caused minimal susceptibility artifacts could be used for implant surgery of the monkey's head fixation system, all materials that were considered for implantation, including skull screws, polyetheracrylate cements and head bolts, were tested prior to surgery. The materials were placed on top of an 11.5 cm cylindrical water container, which will be referred to as a "phantom", while acquiring echo echo-planar (EPI) images (2.5 mm × 2.5 mm × 2.0 mm, FOV = 160 mm × 160 mm; 64 × 64 matrix; TR = 2000 ms, TE = 31 ms, flip angle = 90°). The coronal slice image showing the largest susceptibility artifact for each material was chosen, and each artifact's diameter was measured. For example, Fig. 1A shows a coronal slice through the phantom when a ceramic screw custom manufactured and composed of zirconium dioxide ($ZrO_2 + Y_2O_3$; Ceramco Inc., Center Conway, NH, USA) or a titanium skull screw was placed on top of it with the screw's long axis parallel to the main magnetic field. The artifact that resulted from the ceramic screw reached a maximum depth of 1 cm into the phantom across all slices, whereas the artifact caused by the titanium screw reached a 2 cm depth. These results confirm those of Matsuura et al. (2002) who performed similar tests and found that zirconia ceramic produced a considerably smaller artifact than alumina ceramic, titanium and stainless steel. A polyetherimide head bolt (Model CILUX FHP/D-J9; Crist Instrument Inc., Damascus, MD, USA) caused an artifact that

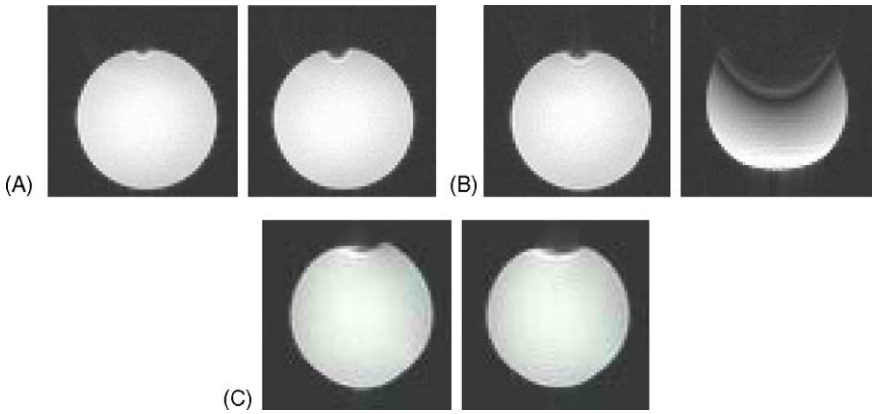

Fig. 1. Material testing for implant surgery. (A) EPI tests revealed a susceptibility artifact that was smaller for a ceramic skull screw (left) in comparison to a titanium skull screw (right). Each screw was 8 mm in length and placed on top of an 11.5 cm diameter cylindrical phantom. Susceptibility artifacts are visible as drops in signal intensity and distortions in the image thereby causing "shadows". (B) EPI tests revealed a much smaller susceptibility artifact for a polyetherimide head bolt (left) in comparison to a titanium head bolt (right). Each cylindrical bolt was approximately 2.5 cm × 1.8 cm. (C) EPI tests of a 100 ml of hardened dental cement (left) in comparison to an alternative bone cement (right) placed on top of a phantom revealed similarly sized artifacts. The blocks of cement were 6 cm × 10 cm × 3 cm.

reached a maximum depth of 1.5 cm, whereas the artifact resulting from the titanium bolt covered half the diameter of the phantom (Fig. 1B). Two different cement materials were tested: dental cement (Cross-Linked Flash Acrylic; Yates & Bird Co., Chicago, IL, USA) and bone cement (Dough-Type Bone Cement; Zimmer Inc., Warsaw, IN, USA). The artifacts caused by both cements were comparable and reached a maximum depth of 1.5 cm (Fig. 1C).

Based on our tests, we chose ceramic screws and dental cement for implant surgery of a polyetherimide head bolt to restrain the animal's head. Due to the susceptibility artifacts caused by the cement some groups avoid using cement for head implants at all and use a more costly polyetherimide head cap machined to conform to the skull's surface (Dubowitz et al., 1998; Logothetis et al., 1999; Vanduffel et al., 2001). Others have opted not to use surgically implanted head restraints, and instead use a cushioned head frame and ear bars under local anesthesia to secure the head (Andersen et al., 2002). To reduce susceptibility artifacts related to our implant method, data acquisition parameters were modified in several respects. Local field inhomogeneities were reduced with localized automatic shimming (Mao and Kidambi, 2000; Reese et al., 1995). A high spatial resolution was used to reduce partial volume effects (Young et al., 1988; Frahm et al., 1993). And scanning was performed at a higher bandwidth to decrease sampling time and $T2^*$ decay (Schmitt et al., 1998).

3.2. MR-compatible primate chair, head-holding apparatus, and RF-coil

Due to the horizontal bore of the Allegra scanner, we designed an MRI primate chair that allows the animal to sit comfortably prone with his head erect ("sphinx" position; Fig. 2) while being head restrained. The chair and head restraint design were constrained by the small diameter (33 cm) of the Allegra scanner bore. The chair was constructed entirely from MR-compatible materials. It consists of a large cast acrylic tube (62 cm length and 28 cm diameter), with front and rear plates made of polycarbonate secured with nylon screws. The size of the tube leaves sufficient space to fit a variety of extra equipment (e.g. juice tubes, coil cables, etc.). A flat surface composed of delrin and polycarbonate was created along the bottom of the tube for the animal to sit upon. This bottom surface contains drainage holes for solid and liquid waste to drop to the bottom of the tube, and also has an inclined front end to help support the animal's chest while sitting in the sphinx position (Fig. 2B). The front cover plate has an opening from which the animal's head protrudes and is held in place with two adjustable polycarbonate neck plates built to each animal's neck size (Fig. 2K). In addition to holding the neck plates, the front plate also contains a small clamp to secure a sipper tube by the animal's mouth (Fig. 2H). A polyethylene cradle was built to secure the chair during positioning of the animal into the chair. A platform with wheels is used to transport the primate chair and cradle to the laboratory and scanner.

A head restraint system made of delrin was conformed to and attached along the top of the inner surface of the tube. This design allowed for the use of a larger diameter tube to accommodate larger animals. The head restraint provides rigid fixation of the animal's head by securing a polyetherimide head post attached to the surgically implanted head bolt. During the course of chair development we found that a single crossbar holding the head post with a couple of pins to prevent head rotations, as used by others (Stefanacci et al., 1998; Vanduffel et al., 2001, Crist Instruments Co., Damascus, MD), was not sufficiently strong to prevent small rotations. Our head restraint system also includes a support bracket fixed along the top inner surface of the chair and protruding through the front above the animal's head (Fig. 2C) that holds the head post holder. The head post holder is adjustable, consisting of two parts, and functions as a clamp to secure the head post. The back part of the head post holder is secured to the support bracket with nylon screws and dovetails (Fig. 2D). The front part slides into place using dovetails along the support bracket, and is secured to the back part with nylon screws to surround the head post (Fig. 2E). The front part also acts as a stabilizing bar for the entire system by attaching to two support pillars on each side of the chair's front plate (Fig. 2G). Two delrin pins in the front and back ends of

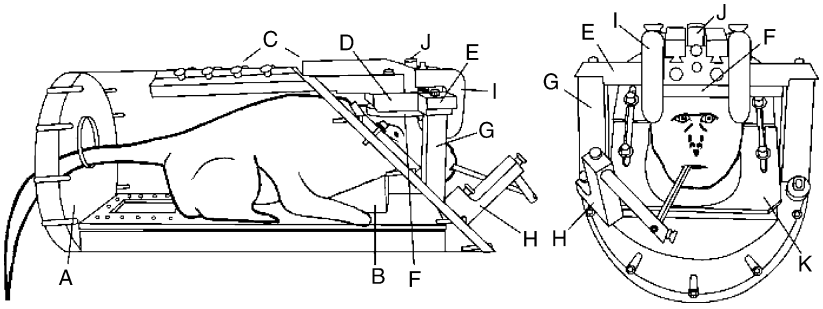

Fig. 2. MR-compatible primate chair. Schematic drawing of side and front views of the primate chair. The chair is constructed of entirely MR-compatible materials (cast acrylic and delrin). Note how the animal is positioned in the "sphinx" position so that stimuli can be displayed directly in front of it. The main components of the chair are labeled (see Section 3 for details). (A) rear panel plate; (B) chest support; (C) head support bracket; (D) back head post holder; (E) front head post holder; (F) surface coil; (G) support pillar; (H) sipper tube holder; (I) plastic C-clamps to hold surface coil; (J) polyetherimide head post; (K) adjustable neck plate.

the head post prevent left/right head rotations. Such a head restraint system provides flexibility when using animals of different sizes, while at the same time rigidly holding their heads in place.

Anatomical and functional images were acquired using a 12-cm transmit/receive surface coil (Model NMSC-023; Nova Medical Inc., Wakefield, MA, USA), which is positioned above the animal's head like a "halo" (Fig. 2F). The coil is secured to the head restraint system of the primate chair with two plastic C-clamps (Duraclamp 476; Burlingham International Inc., Costa Mesa, CA, USA) (Fig. 2I).

3.3. Mock scanner setup and scanner setup

A mock scanner environment was created for animal training (Fig. 3). To habituate the animals to confined spaces, a wooden and polyethylene model of the scanner bore was built to scale. The chair easily slides into the mock bore and is secured with rubber stoppers. Loudspeakers were placed above the mock bore to play scanner noise during training. After the animal was habituated to spend 2–3 h inside the mock bore, recorded scanning noise was played that started at low volumes and gradually increased to the actual scanner volume level (115 dB) over the course of several weeks of training. A single-channel analog video motion detector (MD 2001; Pelco Inc., Clovis, NY, USA) was used to monitor the animal's body movements by placing a video camera at the "tail" end of the mock bore (Fig. 3A). Due to the transparency of the primate chair, the camera is able to pick up body movements that can adversely affect data quality during actual scanning (Birn et al., 1998, 1999). If a movement was detected during training, the trial was aborted instantly. The sensitivity of the motion detector was gradually increased to detect smaller movements. Interestingly, from our experience thus far, it appears that fully trained animals remain very still when engaged in a demanding task, and that there was no need to disregard data due to body movement once the animals were being scanned. An infrared-sensitive camera and LED illuminator was attached to the front of the mock bore to track eye movements at 60 Hz (RK-416; Iscan Inc., Cambridge, MA, USA) (Fig. 3B). During training, visual stimuli were displayed on a CRT monitor placed in front of the mock bore, 60 cm from the animal's eyes (Fig. 3C). A long-range juice delivery system was created so that the pump mechanism could be placed in a control room outside the training room (and also outside the MRI scanner room to prevent electronic interference). This reward system consists of an electronic infusion pump (PHD 2000; Harvard Apparatus Inc., Holliston, MA, USA) that sends juice from a syringe through polyethylene (PE) tubing to a small sipper tube that is mounted to the front plate of the primate chair and inserted into the monkey's mouth (Fig. 2). The stimulus display, motion detection, eye tracking, and reward delivery systems were all computer-controlled with CORTEX software (NIMH, Bethesda, MD, USA).

The setup at the scanner site is in many respects similar to the mock setup in the animal laboratory. Whereas in the mock setup the primate chair is secured with rubber stoppers between the chair and the inside surface of the mock bore, a more rigid system for mounting the primate chair to the patient bed of the scanner was created. The primate chair is mounted to the patient table in the front with a delrin cradle that attaches to both the patient table and the primate chair with nylon screws. The back of the primate chair is secured with two delrin clamps that attach to each side of the chair with nylon screws and hook into the sides of the patient table. A rigid mounting system is important for several reasons. First, such a system will reduce chair movement that occurs when the animal moves. Second, securing the chair to the patient bed prevents the chair from contacting the inner surface of the magnet bore, thus partially isolating it from gradient vibrations that may irritate the animal and degrade image quality. Third, the chair mount allows the chair to be positioned in exactly the same location for each scan session, thereby permitting the same exact slice prescriptions to be acquired since the animal's head is also fixed in the same position. With the same exact slice prescription, we are able to register the slices across sessions for analysis without having to transform the data to a standard template.

The stimulus display is accomplished in the same manner as in the mock setup, except instead of a CRT at the end of the bore, a translucent projection screen displays the stimuli from a digital projector. As in the mock setup, a motion detection camera is placed at the "tail" end of the patient table. The camera is specifically designed for the MR environment (Avotec Inc., Stuart, FL, USA) being magnetically shielded

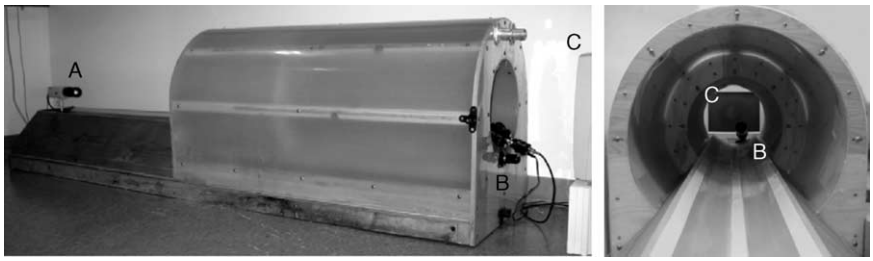

Fig. 3. Mock scanning environment used for animal training. The internal dimensions of the mock bore match the actual scanner bore dimensions. Loudspeakers above the mock bore (not shown) play scanner noises during training. Left panel: side view of the mock bore. Right panel: view inside the bore from the end where the motion-detecting camera is located. (A) Motion-detecting video camera on "tail" end of bore. (B) Eye-tracking camera. (C) Stimulus display monitor.

and having fiber optics to prevent radio frequency interference. A long-range infrared eye tracking system (504 LRO; Applied Science Laboratories Inc., Bedford, MA, USA), capable of measuring the eye position at a rate of 240 Hz with an accuracy of 0.5° and a resolution of 0.25° is located 7 ft from the "head" end of the bore and tracks the animal's eye through a small (4 cm diameter) hole cut in the lower left quadrant of the stimulus display screen. As mentioned above, the juice delivery system remains completely outside the scanner environment with the PE tubing entering through a small opening on the wall into the scanner room (waveguide) to deliver juice to the animal.

3.4. Monkey training

A training procedure was developed to accustom the animals to the chair and scanning environment, and to train them to fixate for extended periods of time in order to perform controlled visual experiments. In a first phase of the training, monkeys were trained for about a week to crawl into the primate chair through the back opening. In a second phase lasting about a week, the animals were habituated to the mock scanner environment by just sitting in the mock bore, listening to the gradient noise and receiving juice every few minutes. A third phase of training was specific to the purpose of our studies that are currently directed at the visual system. The monkeys were trained to fixate a central fixation point for several minutes while stimuli were presented at various locations in the visual field. During this phase of the training the animals were water scheduled to achieve behavioral control using operant conditioning. There were two major reasons for training the animals to fixate for an extended period of time. First, stable fixation allows for controlling stimulus location on the retina, which is important in many visual experiments such as retinotopic mapping (e.g. Brewer et al., 2002; Fize et al., 2003). Second, by having the monkeys fixate for long periods, we can present multiple stimuli in series to increase the power of statistical image analyses.

Fixation times of several minutes were achieved by rewarding the animals with juice at regular intervals ("inter-juice interval", IJI) during fixation trials when their gaze remained within a square window of 4°. To simulate scanning conditions, fixation trials were presented in blocks with several minutes of rest in between. During the first step of this training phase the IJI was gradually increased from 500 ms to 2000 ms. After several weeks of such training, the animals were typically able to fixate for periods of 20–30 s while receiving juice every 2 s. Once the animals achieved peak fixation trials of about 30 s, the training proceeded to a second stage during which the IJI was reduced in 500 ms increments after longer periods of fixation in order to motivate the animal to maintain fixation. For example, after fixating for 30 s, the IJI would be reduced to 1500 ms for the next 30 s of successful fixation, and then again the IJI would be further reduced to 1000 ms for as long as the animal maintained fixation. By introducing this scheme of increasing reward rates achieved

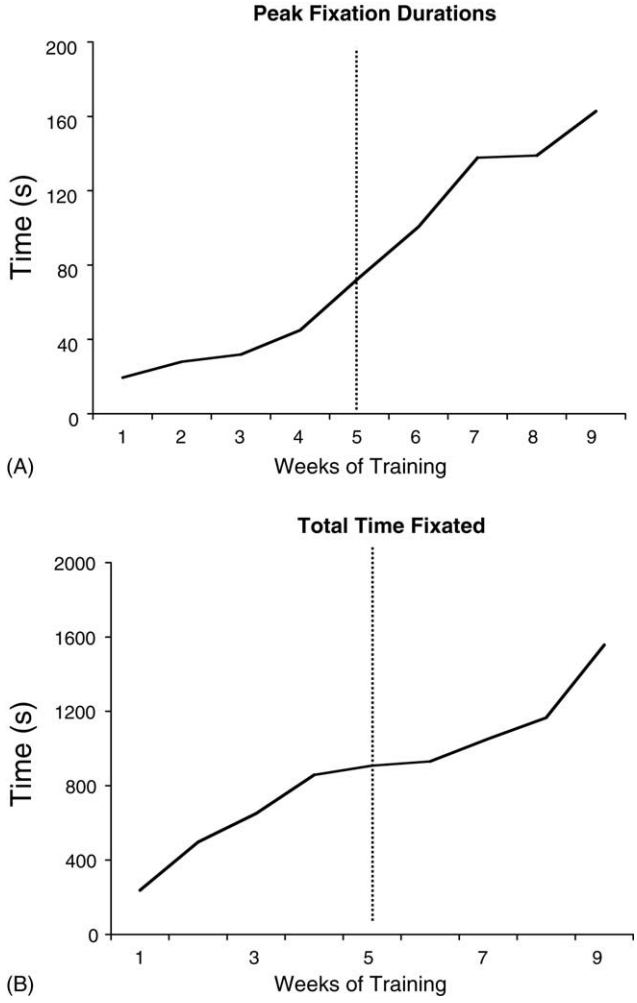

Fig. 4. Fixation training in one animal (M3). (A) Average length of peak fixation trials across daily training sessions. Training is performed in 4 min blocks interleaved with equally long rests. After 9 weeks, the animal could fixate for about 3 min. The longest fixation trial that the animal performed in each of seven consecutive training sessions was averaged. (B) Total amount of time that the animal spent fixating in each training session. After 9 weeks, the animal fixated for about 30 min per session. Data were averaged using 7-day bins. The vertical dotted line indicates the time when inter-juice intervals decreasing in a predictable manner were introduced.

by reducing IJI's in predictable ways, we were able to increase the lengths of fixation trials significantly (dotted line, Fig. 4, Monkey M3). Once the animals became familiar with this reward scheme, it was fairly easy to gradually extend the times between IJI decreases in order to prolong the overall duration of fixation trials. After a couple of months of daily training the duration of fixation trials approached 3 min (Fig. 4A), while the overall fixation time per training session reached a total of 27 min (Fig. 4B). During a training session the animals typically performed 8–10 blocks of 4 min each, interleaved with rest periods of 4 min to simulate the timing parameters of an actual scanning session closely. During the fixation trials, the animals were allowed to blink and make brief eye movements leaving the fixation window as long as the eye returned to the fixation spot within less than 200 ms.

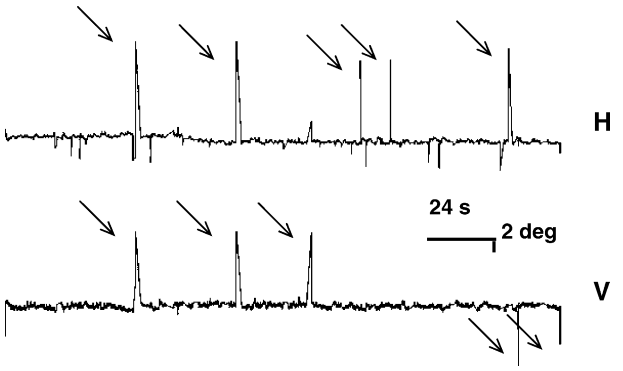

Fig. 5. Eye position recordings from animal M1. Horizontal (H) and vertical (V) eye traces from a representative trial lasting 3 min. Eye positions were recorded using an MR-compatible infrared eye tracker (ASL Co.). Arrows indicate eye movements outside the 4° square fixation window. The animals were trained to return to the fixation spot after an eye blink or small eye movement within 200 ms, otherwise the trial was aborted.

Such brief eye movements were infrequent events, as can be seen in the representative eye trace in Fig. 5. Eye blinks were eliminated by applying a pupil size and location filter (ILAB v. 3.57, Gitelman, 2002). It is important to note that the size of the animal will affect the amount of juice reward and, therefore, strongly influence the total amount of time it can fixate during a session. A trained animal weighing 6–9 kg will typically receive ∼25 ml of juice reward during a 3 min scan or training period, and will complete 8–10 scans in a session, amounting to a total of 200–250 ml of juice reward. Other laboratories performing fMRI in awake monkeys have reported similar training schemes to achieve long fixation durations (Vanduffel et al., 2001; Tsao et al., 2003a).

3.5. Anatomical scanning

For each animal, an anatomical scan (MPRAGE sequence, 20 repetitions that were averaged, for scanning parameters, see Section 2) of 0.5 mm × 0.5 mm × 0.5 mm spatial resolution was acquired in a single scanning session, during which the animals were anesthetized. These images were used for surface reconstructions of the monkey's cortex. Although the number of acquisitions necessary to obtain sufficient signal for accurate segmentation was not formerly investigated in this study, our experiences have shown that with a surface coil, 15–20 scans were necessary to gain a sufficient signal-to-noise ratio in regions of the brain that were distant to the coil such as inferior temporal cortex. Surface reconstructions with fewer acquisitions may yield similar results, but will require more manual intervention when segmenting the surface. Due to the use of a surface coil, the original structural images exhibited a gradient in signal intensity that was brightest closest to the coil (i.e. the top of the head) and decreased towards the bottom of the head, as distance from the coil increased (Fig. 6A). Because the cortical segmentation algorithms implemented by surface reconstruction software rely largely on image intensity values to distinguish brain tissue (i.e. gray matter (GM), white matter (WM), cerebral spinal fluid (CSF)), a gradient in signal intensity defeats these algorithms. Therefore, a non-uniform intensity correction (NUC) algorithm was applied. Based on the results of Arnold et al. (2001) who systematically assessed the performance of various NUC algorithms on real and simulated MRI data from a volume coil, we chose to use the *n3* algorithm (Sled et al., 1998) rated as one of the top performing ones. Whether this algorithm outperforms the others on extremely non-uniform data collected with a surface coil remains to be studied. For our purpose of segmenting the cortical surface, the *n3* algorithm proved sufficient. As noted by Arnold et al. (2001), it is unknown whether NUC algorithms perform better when non-brain regions (i.e. skull and muscles) are masked first. We chose to remove non-brain tissue after applying the *n3* algorithm since the skull removal software (Smith, 2002) performed best once the volumes were intensity corrected. In addition, to further improve the images for tissue segmentation, the images were de-noised with a non-linear filter that preserved the underlying structural information in the images (Smith, 1996) (Fig. 6B).

The resulting brain volumes were segmented and the cortical surfaces were reconstructed. Software for automatically segmenting and reconstructing the cortical surface has been developed using different techniques by several laboratories in the past years (Teo et al., 1997; Dale et al., 1999; Fischl et al., 1999; Van Essen et al., 2001). These techniques are often used in human imaging studies, and are now beginning to be applied in monkey fMRI studies (Brewer et al., 2002; Tsao et al., 2003a,b; Orban et al., 2003). Using the SureFit software package developed by Van Essen et al. (2001), the cortical surface representing layer 4 was segmented, reconstructed and imported into the Caret software package for the creation of additional surfaces and atlas registration (Van Essen et al., 2001; Van Essen, 2002, 2004) (Fig. 6C). After spherical surfaces were created, a macaque brain atlas was warped to the individual surface using spherical-based registration techniques that rely on anatomical landmarks such as the major sulci to constrain the deformation. This warping was applied to the flattened surfaces, thereby allowing for a variety of area borders from previous mapping studies to be projected onto the individual surface and providing a general framework of the location of functional activity relative to anatomical landmarks. An example is provided in Fig. 6D where area borders in ventral temporal cortex are based on Ungerleider and Desimone's (1986) and dorsal cortical regions are delineated using Felleman and Van Essen's (1991) partitioning scheme.

For the monkey with the unilateral striate lesion (monkey M4), the extent of the lesion was assessed by examining anatomical scans before and after surgery. Fig. 7A shows T1-weighted anatomical images of the lesioned right hemisphere of M4 from a coronal view along with corresponding line drawings. The lesion extended laterally from the occipital pole removing striate cortex on the occipital gyrus and stopping 2 mm posterior to the

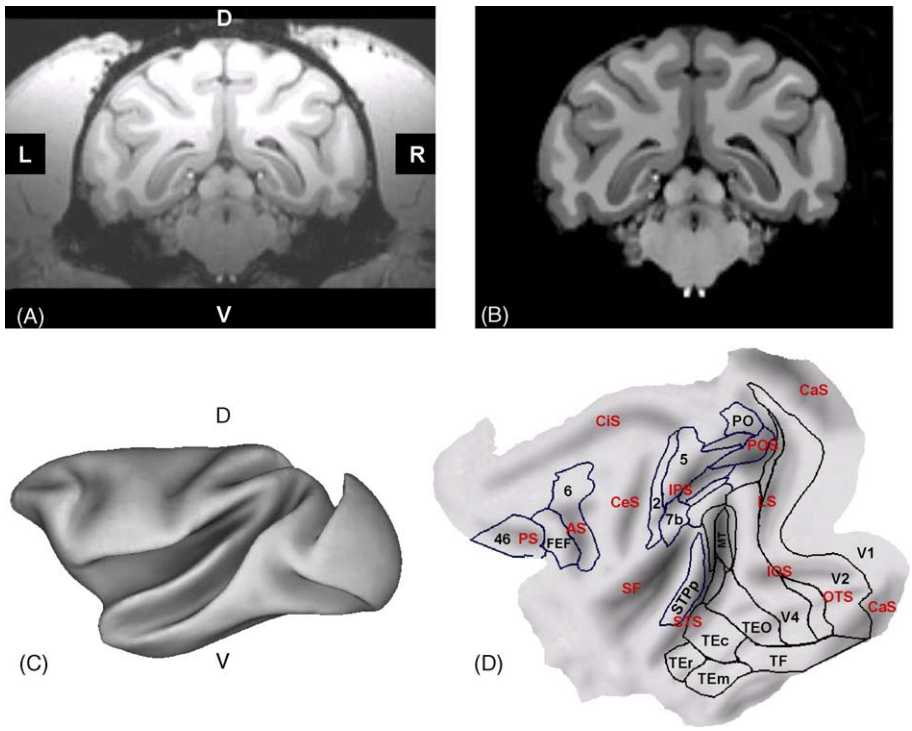

Fig. 6. Anatomical scanning and surface reconstructions. High-resolution (0.5 mm × 0.5 mm × 0.5 mm) anatomical scans were acquired to create cortical surface reconstructions. (A) A sample image slice of the original anatomical scan. Note the gradient in signal intensity that increases with distance from the surface coil, located dorsally along the top of the head. (D: dorsal, V: ventral, L = left, R: right.) (B) The same sample image slice after the volume has undergone several pre-processing steps to improve the tissue contrast and reduce the signal gradient. (C) A lateral view of the surface of a segmented left hemisphere. The surface has been inflated to open up the sulci. (D) A flattened left hemisphere with area borders from previous mapping studies deformed and projected onto it. The relative brightness of the surface indicates the surface depth, where black regions are the fundi of the sulci. Major sulci are labeled in red and are abbreviated as follows: CiS: cingulate sulcus; CeS: central sulcus; IPS: intraparietal sulcus; POS: parieto-occipital sulcus; CaS: calcarine sulcus; LS: lunate sulcus; IOS: inferior occipital sulcus; OTS: occipito-temporal sulcus; STS: superior temporal sulcus; SF: sylvian fissure; AS: arcuate sulcus; PS: principal sulcus. Dorsal and ventral area boundaries are delineated with solid lines and labeled according to the partitioning schemes from Felleman and Van Essen (1991) and Ungerleider and Desimone (1986), respectively.

lateral end of the lunate sulcus, likely in the vicinity of the foveal representation of V1 (Gattass et al., 1981). On the medial side, the lesion extended from the occipital pole 5 mm anterior into the calcarine sulcus. The total area of ablated cortex corresponded to the central 8–12° of the visual field (Gattass et al., 1981). Cortex along the posterior bank and convexity of the inferior occipital sulcus and lunate sulcus remained intact. The anterior border of the lesion corresponded approximately to the representation of the vertical meridian border in V1 (Gattass et al., 1981). To create a surface reconstruction of the hemisphere with the lesion, the cortex surrounding the lesion had to be defined manually. Intact cortex surrounding the lesion was determined to be either gray or white matter through visual inspection of the image in the three cardinal viewing planes, and interactively edited using the SureFit software package.

Once this process was performed on a slice-by-slice basis in all three viewing planes, the final surface representing cortical layer 4 was created. The surface was linked back to the original image slices, visually inspected for accuracy, and re-edited if necessary until the surface accurately represented the extent of the lesion. The resulting surface reconstruction is shown in Fig. 7B.

3.6. Functional scanning: visually-evoked activity during free viewing

After the animals had completed phase 2 of the training, functional baseline scans were acquired for three normal monkeys and one monkey with a unilateral striate lesion. In a single session, monkey subjects were presented under free viewing conditions with 30 s clips of an animated movie alternating with blank presentations of the same length. Each scan lasted for 210 s and was repeated six times.

Activity patterns of visual stimulation epochs compared to blank intervals are depicted in Fig. 8 A on flattened reconstructions of the cortical surface for right and left hemispheres of monkey M1 ($z > 3.72$, $p < 0.0001$). Common active regions in early visual cortex included striate cortex within the calcarine sulcus (CS) and the lateral surface of the occipital gyrus. Activity was also found in ventral extrastriate cortex within and around the lunate sulcus, the inferior occipital sulcus, the posterior end of the occipito-temporal sulcus, and the middle and inferior temporal gyri. Dorsal extrastriate areas were activated including regions around the parieto-occipital sulcus, the intraparietal sulcus (IPS), and the posterior end of the superior temporal sulcus (STS). In addition, a

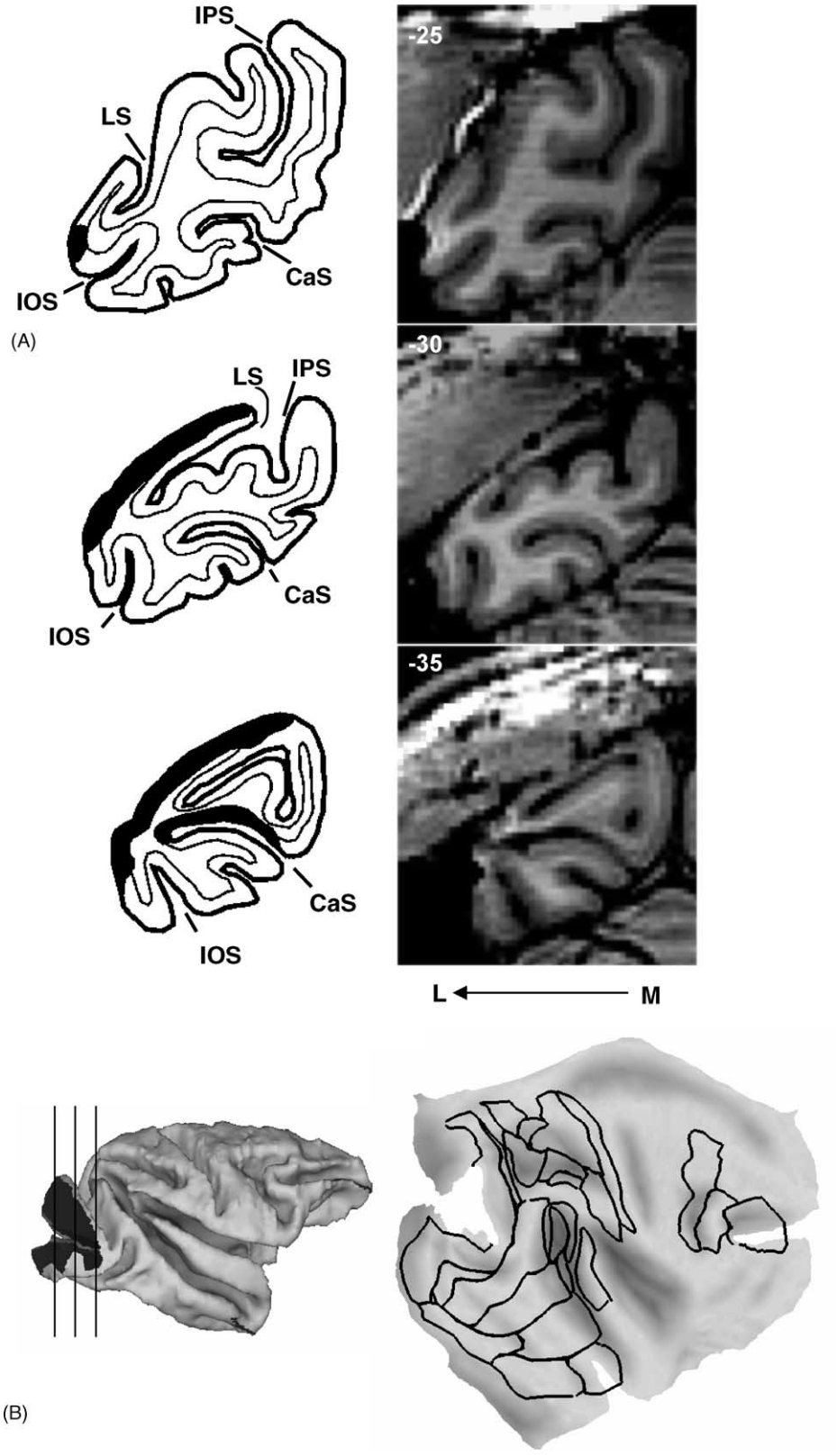

Fig. 7. Anatomical scans and surface reconstructions of the lesioned right hemisphere of animal M4. (A) Line drawings and matching T1-weighted anatomical scans of occipital cortex two months post-surgery. Coronal slices of the right hemisphere are shown. Each slice is approximately 5 mm apart. Numbers in the left-hand corner indicate distance from the anterior commissure. Major sulci are labeled on the line drawings, same abbreviations as in Fig. 6; L: lateral, M: medial. (B) The surface reconstruction of the lesioned hemisphere shown as a folded surface (left) and a flattened surface (right). Approximate locations of the slices shown in (A) are marked with vertical lines through the folded surface reconstructions.

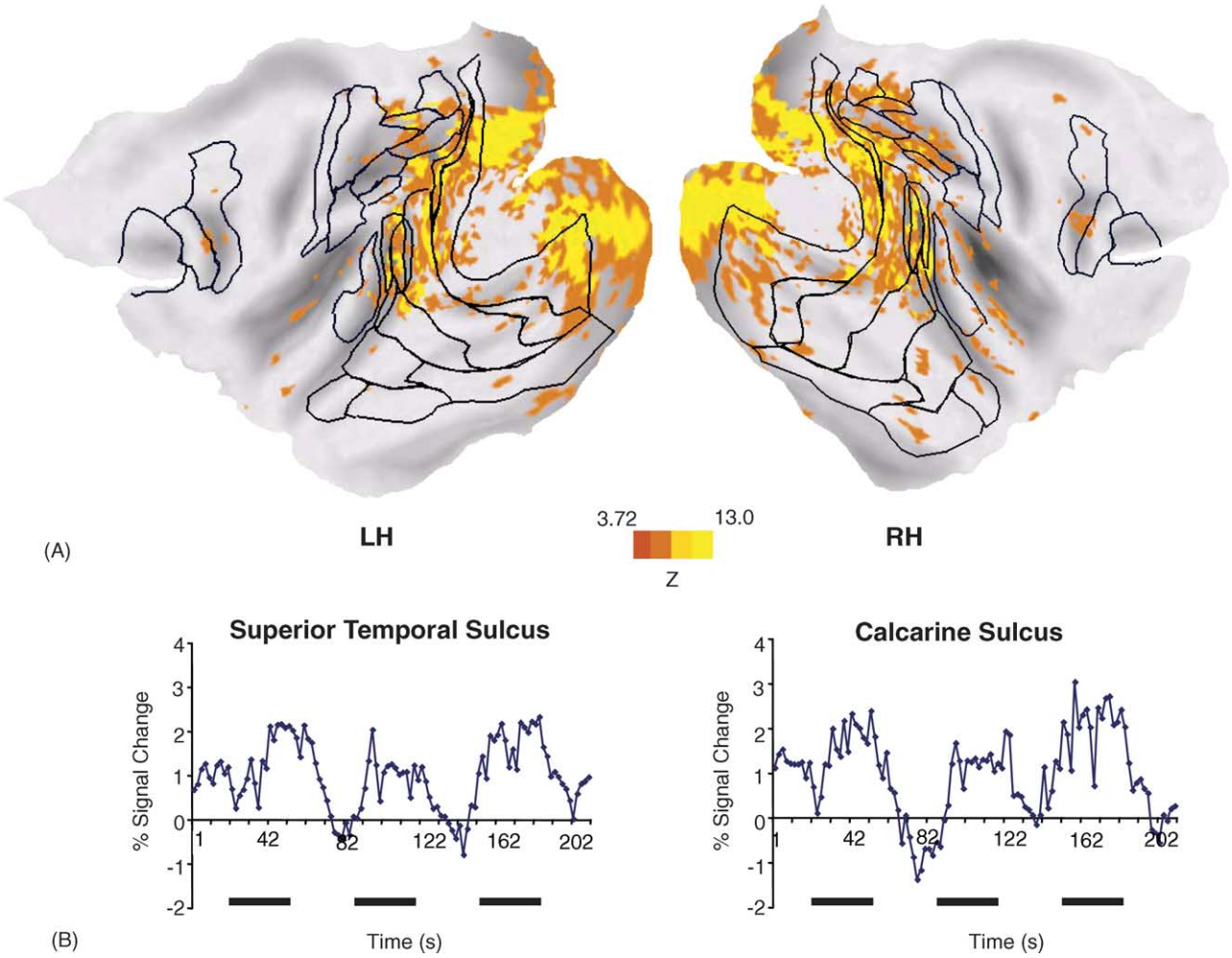

Fig. 8. Visually-evoked fMRI activity during free viewing. (A) Flattened left (LH) and right (RH) hemispheres of a normal monkey (M1). Activity related to viewing clips of a cartoon movie has been painted onto the surfaces revealing bilateral activation in striate and extrastriate visual cortex, parietal cortex and frontal regions near the arcuate sulcus. Area borders as shown in Fig. 6 have been deformed to the individual surfaces. Activations were consistent across hemispheres and monkey subjects. Scale indicates *z*-score values of activations in colored regions. (B) Time courses of fMRI signals in two anatomically defined regions (right calcarine sulcus [95 voxels] and right superior temporal sulcus [121 voxels]) are shown. Signals were not smoothed and were averaged across six scans; they reflect the three epochs of visual stimulation (black bars) interleaved with blank periods. Color bar indicates *z* values.

frontal region that included the arcuate sulcus and the frontal gyrus was activated. The activity tended to be symmetrical across both hemispheres. Similar patterns of activity were found in monkeys M2 and M3, and in the non-lesioned hemisphere of monkey M4 (Fig. 9B). The activity patterns were likely a result of both visually-evoked and eye movement-related activity. This is best illustrated by the active regions in the vicinity of the arcuate sulcus and frontal gyrus corresponding to the frontal eye fields (e.g. Bizzi, 1967; Bruce and Goldberg, 1985; Bruce et al., 1985). Further, single cell physiology studies have shown that neural responses across visual cortex can be modulated by eye position (e.g. Andersen and Mountcastle, 1983; Galletti and Battaglini, 1989; Andersen et al., 1990; Weyand and Malpeli, 1993; Galletti et al., 1995; Nakamura et al., 1999).

ROIs from the superior temporal sulcus and calcarine sulcus were selected to examine MR signals more closely. FMRI signals were averaged across all activated voxels ($z > 3.72$, $p < 0.0001$) within a given ROI and across scans, and normalized to the average level of the blank periods. The time courses of the signals were closely linked to the experimental paradigm, with signal increases during the visual stimulation blocks on the order of 2% from baseline, as shown for two ROIs from the superior temporal sulcus and the calcarine sulcus (Fig. 8B).

In monkey M4, the effect of the lesion on the quality of the echo-planar images was assessed. In Fig. 9A, T1-weighted and echo-planar images closely matched to the same axial planes covering the extent of the lesion are shown. The functional activity obtained in the free-viewing experiment is also overlaid on the same EPI images ($z > 3.72$, $p < 0.0001$) (Fig. 9A). Notably, there is a signal drop in the region of the lesion; however, regions in the immediate vicinity of the lesion were activated, as can be seen in the axial echo-planar images. An ROI comprising of the region surrounding the lesioned cortex was selected to examine the MR signals

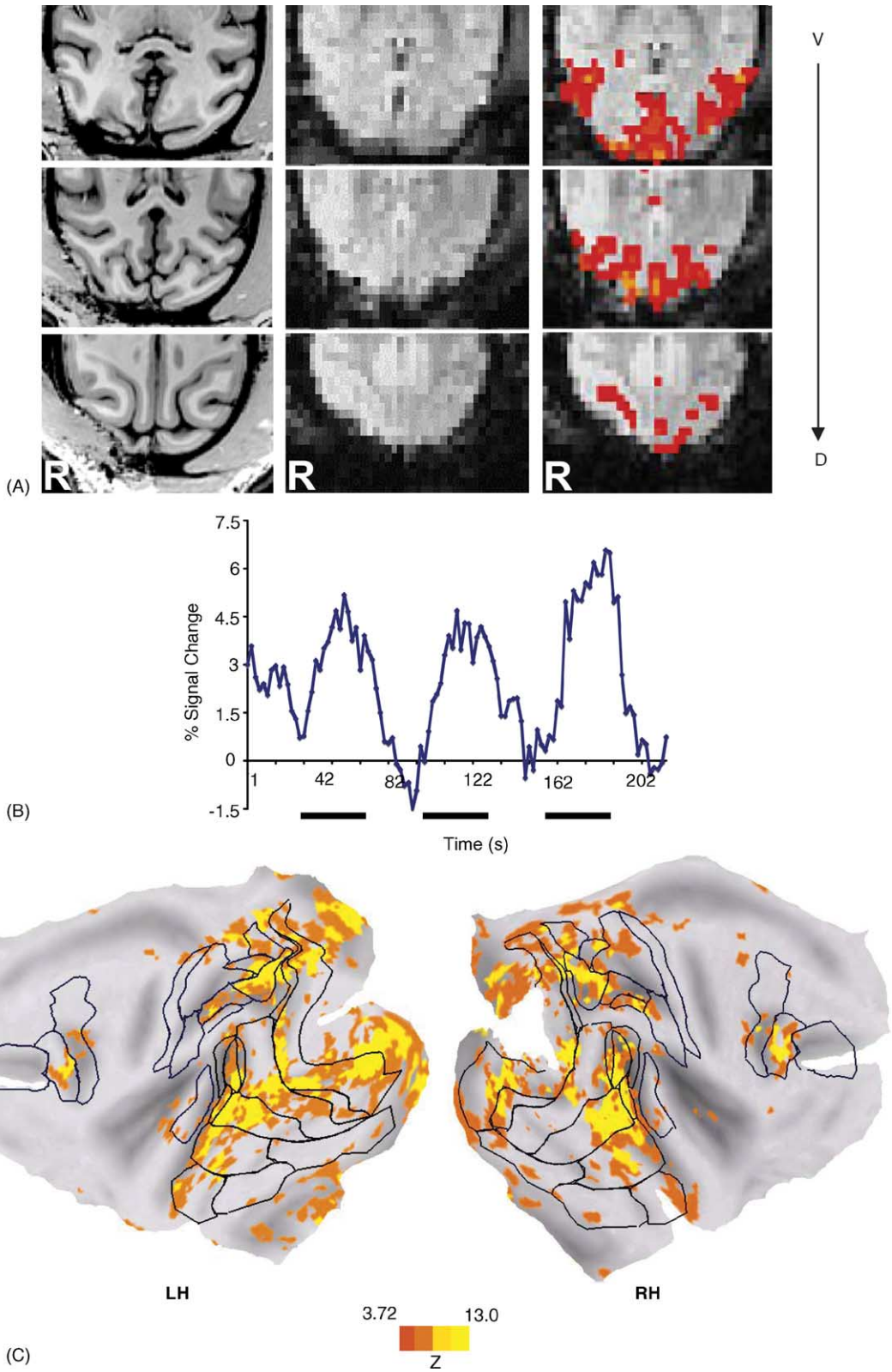

Fig. 9. Visually-evoked fMRI activity during free viewing in a monkey with a unilateral striate lesion. (A) Left-hand column: T1-weighted axial slices (0.5 mm × 0.5 mm × 0.5 mm resolution). The lesion can be seen in the right hemisphere. Middle column: EPI axial slices (1.25 mm × 1.25 mm × 2.0 mm resolution) closely matched to the T1-weighted slices. Right-hand column: same axial slices as in middle column, but with significantly activated voxels related to viewing the cartoon stimulus overlaid upon them ($z > 3.72$, $p < 0.0001$). (B) Time course of fMRI signal in statistically significant voxels immediately adjacent to the lesion [84 voxels] are shown. Signals were not smoothed and were averaged across six scans; they reflect the three epochs of visual stimulation (black bars) interleaved with blank periods. (C) Flattened surface reconstructions of the left and right hemispheres of the lesioned monkey. Activity related to freely viewing the cartoon stimulus has been painted onto the surfaces. Other conventions as in Figs. 6 and 8.

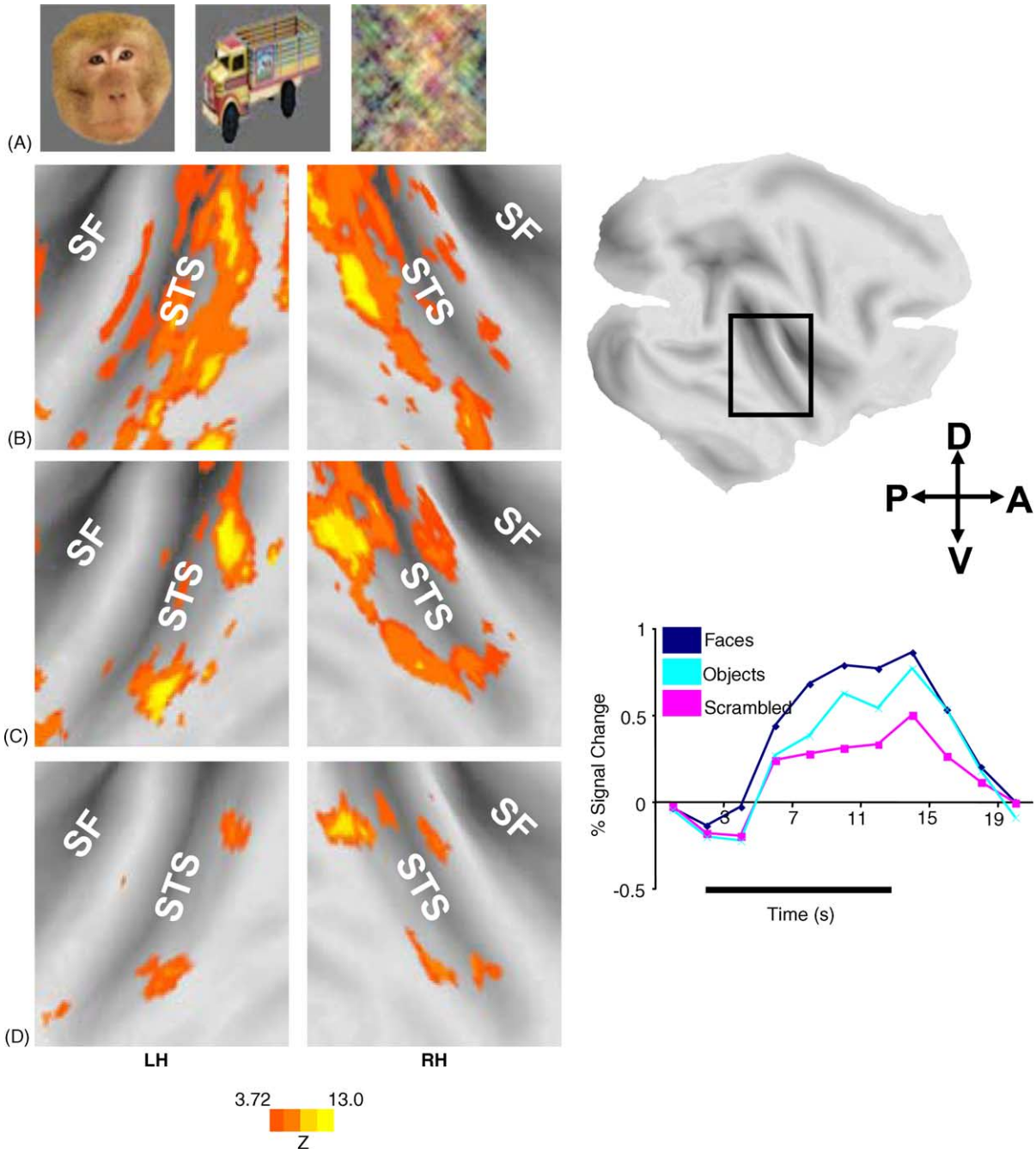

Fig. 10. Face-selective regions in monkey visual cortex. (A) Visual stimuli were presented foveally while the monkey maintained fixation. Three categories of stimuli were used: faces, objects, scrambled pictures. (B–D) Close-up views of flattened left and right hemispheres of monkey M2. The location of the close-up views with respect to an entire flattened hemisphere is shown on the right. (B) Voxels activated significantly more by intact objects compared to scrambled pictures are painted onto the surfaces. (C) Voxels activated significantly more by faces compared to scrambled pictures are painted on the surfaces. (D) Voxels activated significantly more by faces compared to intact objects are painted onto the surfaces. Time courses of fMRI signals from the face-selective region in the posterior STS are shown to the right. Signals were not smoothed and were averaged across similar conditions; each line reflects the fMRI signal from a different condition. Dark blue: face condition; light blue: object condition; pink: scrambled condition. Black bar: duration of visual stimulation epoch. Similar results were found in a second monkey (M1), not shown here. STS: superior temporal sulcus; SF: sylvian fissure; D: dorsal; V: ventral; P: posterior; A: anterior.

more closely. FMRI signals were averaged across all activated voxels ($z > 3.72$, $p < 0.0001$) bordering the lesion and across scans, and normalized to the average level of the blank periods. The time course of the signals were closely linked to the experimental paradigm, with signal increases during the visual stimulation blocks on the order of 4.5% from baseline, as shown in Fig. 9B. The activated regions in the vicinity of the lesion are also visible on the surface reconstruction (Fig. 9C). Activated regions included the calcarine sulcus, lunate sulcus and inferior occipital sulcus. These results suggest that the

lesion surgery did not compromise image quality and BOLD contrast in regions immediately adjacent to the lesioned cortex.

3.7. Functional scanning: face- and object-related activity during fixation

After the animals had completed phase 3 of the training, functional scans were acquired while the animals performed the fixation task. Pictures of human and monkey faces, man-made objects, and phase-scrambled pictures were presented in alternation with blank presentations (for examples of stimuli, see Fig. 10A). Data from several sessions of 8–10 scans each were combined for analysis (see Section 2).

Activity evoked by intact objects versus scrambled pictures, faces versus scrambled pictures, and faces versus intact objects was compared in monkeys M1 and M2. The first contrast comparing the intact objects to the scrambled pictures revealed large bilateral activations throughout ventral extrastriate cortex including areas from the inferior occipital sulcus to anterior superior temporal sulcus/inferior temporal gyrus (STS/ITG) (Fig. 10B). The second contrast comparing the face stimuli to the scrambled pictures revealed smaller, more selective clusters of activity within the same regions (Fig. 10C). The third contrast comparing the face stimuli to the object stimuli, revealed face-selective activity in two regions: one activated region in the fundus and banks of the posterior STS, and another more anterior region in the middle temporal gyrus (MTG) and STS ($z > 3.72$, $p < 0.0001$) (Fig. 10D). The time course of fMRI signals was examined by averaging across all activated voxels ($z > 3.72$, $p < 0.0001$) within the right posterior STS face area and across scans, and normalized to the average level of the blank periods. Neural responses evoked by faces were stronger than those evoked by objects; activity evoked by scrambled pictures was smallest (Fig. 10). These regions correspond to known locations of face-selective neurons from single cell physiology (Gross et al., 1972; Perrett et al., 1982; Desimone et al., 1984) and face activations found in monkey fMRI studies (Logothetis et al., 1999; Tsao et al., 2003a).

Eye movement analyses confirmed that the animals maintained fixation for most of the time during the scanning sessions. For example, during each of the four sessions that was analyzed monkey M2 maintained fixation within the 4° window for $87 \pm 10\%$, $98 \pm 2\%$, $97 \pm 3\%$ and $95 \pm 3\%$ of the time, respectively. On average, the animal made 20 ± 10, 1 ± 1, 5 ± 7, and 8 ± 7 eye movements outside the window that lasted for more than 500 ms before returning to the window during each 3 min scan in each of the four sessions, respectively. For each session, there were no significant differences in the amount of horizontal and vertical eye movement between the three different categories of stimuli (horizontal eye movements: session 1, $F_{0.05}(2, 45) = 0.47$, $p = 0.62$; session 2, $F_{0.05}(2, 51) = 2.02$, $p = 0.14$; session 3, $F_{0.05}(2, 30) = 0.14$, $p = 0.86$; session 4, $F_{0.05}(2, 25) = 0.16$, $p = 0.85$; vertical eye movements: session 1, $F_{0.05}(2, 44) = 0.53$, $p = 0.58$; session 2, $F_{0.05}(2, 51) = 0.52$, $p = 0.59$; session 3, $F_{0.05}(2, 30) = 1.63$, $p = 0.21$; session 4, $F_{0.05}(2, 25) = 1.28$, $p = 0.29$). Fixation performance of monkey M1 was similar.

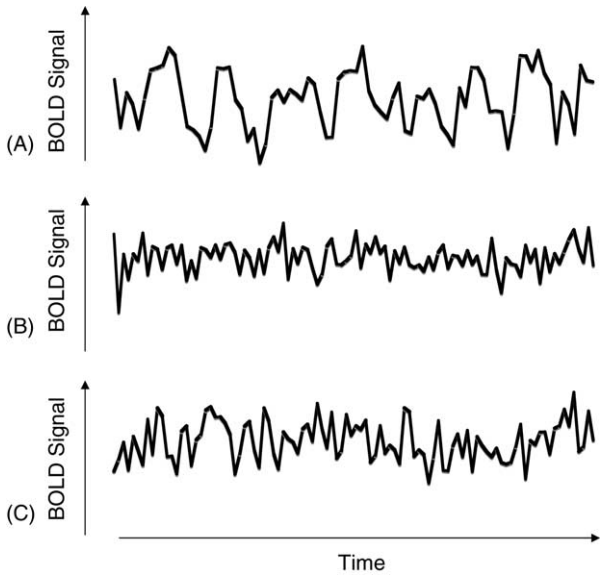

Fig. 11. Effects of reward on fMRI signals. The average signals of eight time series from a single scan session (monkey M2) are shown from a statistically significant activated voxel in visual cortex while regular rewards were provided (A), from a voxel in frontal cortex whose activity was not correlated with the visual stimulation paradigm while regular rewards were provided (B), and from the same voxel as in (B) when regular rewards were not provided (C). Axis scales are identical for (A–C). No reward-related activity or artifacts in the signals were apparent.

To assess whether the administration of rewards during scanning caused artifacts due to mouth movements, we compared the signal of a voxel in frontal cortex that was not significantly correlated with the visual stimulation paradigm from experiment 1 (where the animal did not receive any rewards during the scan) to the signal from the same voxel from experiment 2 (where the animal did receive juice rewards at regular intervals during the scan). As shown in Fig. 11, no reward-related artifacts such as large signal spikes were apparent (Fig. 11B versus C). For comparison, the signal of a single voxel in visual cortex is shown that was significantly correlated with our stimulation paradigm (Fig. 11A). Because the reward was delivered at the same rate or faster as the signal was acquired (2 s), it is possible that the mouth movements caused a steady change in the MR signal throughout the entire scan. If so, such movements will affect each experimental condition in similar ways given that movements were present throughout the scan.

4. Conclusion

In this report, we have described in detail methods for performing fMRI in normal and lesioned awake monkeys. Materials available for head implants were assessed in terms

of susceptibility artifacts; ceramic and polyetherimide materials were found to be the most compatible. A primate chair, mock scanning environment and training procedures were developed to accustom the animals to the scanner and to have them fixate for several minutes in order to perform controlled visual studies. Using a surface coil, whole brain anatomical images were acquired that were of sufficient quality to create cortical surface reconstructions of both normal and lesioned monkeys after non-uniform intensity correction. Our methods were then confirmed by acquiring functional images in two visual experiments—one under free-viewing conditions in both normal and lesioned animals, and another during fixation in trained animals.

One potentially important application of monkey fMRI is to investigate the system-wide recovery of neural function following cortical lesions (Payne and Lomber, 2001). However, to date, there have been no studies examining whether a combination of monkey fMRI and lesion techniques is feasible. There are serious concerns regarding image quality after lesion surgery. Specifically, it is possible that a craniotomy and lesion introduce large susceptibility artifacts that could preclude measuring BOLD signals in the immediate vicinity of the lesion. FMRI studies in human patients after surgery involving craniotomy have indeed shown signal losses in regions of the craniotomy (Jezzard et al., 2001). However, these image artifacts may be due to the use of standard biomaterials that produce susceptibility artifacts, and MR imaging parameters that are not optimized to decrease the sensitivity to magnetic susceptibility. Here, we carefully selected implant materials and imaging parameters to reduce magnetic susceptibility. We then scanned a monkey with a unilateral striate lesion in experiment 1. The extent of the lesion was assessed and reconstructed from T1-weighted anatomical scans acquired with a surface coil. In the EPI images, susceptibility artifacts from the lesion were observed in terms of signal drop out that was restricted to the location of the lesion. Statistically significant activity was found in the immediate vicinity of the lesion. Although future studies using a larger number of animals will have to confirm and extend these results, our findings suggest that studies of recovery of neural function after circumscribed lesions are feasible using fMRI in behaving non-human primates. Such studies will be helpful in better understanding, for example, models of recovery from stroke in which the involvement of surrounding tissue in plasticity is of particular interest (Xerri et al., 1998; Jenkins and Merzenich, 1987).

Acknowledgements

We would like to thank Michael Graziano for help with animal surgery and advice with animal training, and Kevin DeSimone for assistance with animal training and scanning. We are grateful to Jim Watson and Don Forte for building our custom equipment, Michael Benharrosh, Peter Hutter, Ben Singer and Sylvain Takerkart for hardware and software support, Dylan Cooke for assistance taking the stimulus photographs, Jeffrey Gelt for assistance with manuscript preparation, our colleagues at Washington University—David Van Essen, Donna Hanlon, Jon Harwell for their invaluable help using the SureFit and Caret software packages, Kimberly Montgomery and members of the Kastner Lab for valuable discussions, and Jonathan Cohen and James Haxby for their continuing support. This work was supported by NIH grants to C.G.G. (RO1 EY-11347) and S.K. (RO1 MH-64043, P50 MH-62196), a Whitehall Foundation grant to S.K. and an NSF Graduate Research Fellowship to M.A.P.

References

Andersen AH, Zhang Z, Barber T, Rayens WS, Zhang J, Grondin R, et al. Functional MRI studies in awake rhesus monkeys: methodological and analytical strategies. J Neurosci Methods 2002;118(2):141–52.

Andersen RA, Bracewell RM, Barash S, Gnadt JW, Fogassi L. Eye position effects on visual, memory, and saccade-related activity in areas LIP and 7a of macaque. J Neurosci 1990;10(4):1176–96.

Andersen RA, Mountcastle VB. The influence of the angle of gaze upon the excitability of the light-sensitive neurons of the posterior parietal cortex. J Neurosci 1983;3(3):532–48.

Arnold JB, Liow JS, Schaper KA, Stern JJ, Sled JG, Shattuck DW, et al. Qualitative and quantitative evaluation of six algorithms for correcting intensity nonuniformity effects. Neuroimage 2001;13(5):931–43.

Birn RM, Bandettini PA, Cox RW, Jesmanowicz A, Shaker R. Magnetic field changes in the human brain due to swallowing or speaking. Magn Reson Med 1998;40(1):55–60.

Birn RM, Bandettini PA, Cox RW, Shaker R. Event-related fMRI of tasks involving brief motion. Hum Brain Mapp 1999;7(2):106–14.

Bizzi E. Discharge of frontal eye field neurons during eye movements in unanesthetized monkeys. Science 1967;157(796):1588–90.

Brewer AA, Press WA, Logothetis NK, Wandell BA. Visual areas in macaque cortex measured using functional magnetic resonance imaging. J Neurosci 2002;22(23):10416–26.

Bruce CJ, Goldberg ME. Primate frontal eye fields. I. Single neurons discharging before saccades. J Neurophysiol 1985;53(3):603–35.

Bruce CJ, Goldberg ME, Bushnell MC, Stanton GB. Primate frontal eye fields. II. Physiological and anatomical correlates of electrically evoked eye movements. J Neurophysiol 1985;54(3):714–34.

Buxton RB. Introduction to functional magnetic resonance imaging: principles and techniques. Cambridge: Cambridge University Press; 2001.

Cohen MS. Parametric analysis of fMRI data using linear systems methods. Neuroimage 1997;6(2):93–103.

Cox RW. AFNI: software for analysis and visualization of functional magnetic resonance neuroimages. Comput Biomed Res 1996;29(3):162–73.

Cox RW, Hyde JS. Software tools for analysis and visualization of fMRI data. NMR Biomed 1997;10(4–5):171–8.

Cox RW, Jesmanowicz A. Real-time 3D image registration for functional MRI. Magn Reson Med 1999;42(6):1014–8.

Dale AM, Fischl B, Sereno MI. Cortical surface-based analysis. I. Segmentation and surface reconstruction. Neuroimage 1999;9(2):179–94.

Denys K, Vanduffel W, Fize D, Nelissen K, Peuskens H, Van Essen D, et al. The processing of visual shape in the cerebral cortex of human and nonhuman primates: a functional magnetic resonance imaging study. J Neurosci 2004;24(10):2551–65.

Desimone R, Albright TD, Gross CG, Bruce C. Stimulus-selective properties of inferior temporal neurons in the macaque. J Neurosci 1984;4(8):2051–62.

Disbrow E, Roberts TP, Slutsky D, Krubitzer L. The use of fMRI for determining the topographic organization of cortical fields in human and nonhuman primates. Brain Res 1999;829(1–2):167–73.

Dubowitz DJ, Bernheim KA, Chen DY, Bradley Jr WG, Andersen RA. Enhancing fMRI contrast in awake-behaving primates using intravascular magnetite dextran nanopartieles. Neuroreport 2001;12(11):2335–40.

Dubowitz DJ, Chen DY, Atkinson DJ, Grieve KL, Gillikin B, Bradley Jr WG, et al. Functional magnetic resonance imaging in macaque cortex. Neuroreport 1998;9(10):2213–8.

Felleman DJ, Van Essen DC. Distributed hierarchical processing in the primate cerebral cortex. Cereb Cortex 1991;1(1):1–47.

Fischl B, Sereno MI, Dale AM. Cortical surface-based analysis. II: Inflation, flattening, and a surface-based coordinate system. Neuroimage 1999;9(2):195–207.

Fize D, Vanduffel W, Nelissen K, Denys K, Chef d'Hotel C, Faugeras O, et al. The retinotopic organization of primate dorsal V4 and surrounding areas: a functional magnetic resonance imaging study in awake monkeys. J Neurosci 2003;23(19):7395–406.

Frahm J, Merboldt KD, Hanicke W. Functional MRI of human brain activation at high spatial resolution. Magn Reson Med 1993;29(1):139–44.

Friston KJ, Frith CD, Frackowiak RS, Turner R. Characterizing dynamic brain responses with fMRI: a multivariate approach. Neuroimage 1995;2(2):166–72.

Galletti C, Battaglini PP. Gaze-dependent visual neurons in area V3A of monkey prestriate cortex. J Neurosci 1989;9(4):1112–25.

Galletti C, Battaglini PP, Fattori P. Eye position influence on the parieto-occipital area PO (V6) of the macaque monkey. Eur J Neurosci 1995;7(12):2486–501.

Gattass R, Gross CG, Sandell JH. Visual topography of V2 in the Macaque. J Comp Neurol 1981;201:519–39.

Gitelman DR. ILAB: a program for postexperimental eye movement analysis. Behav Res Methods Instr Comp 2002;34:605–12.

Gross CG, Rocha-Miranda CE, Bender DB. Visual properties of neurons in inferotemporal cortex of the Macaque. J Neurophysiol 1972;35(1):96–111.

Jenkins WM, Merzenich MM. Reorganization of neocortical representations after brain injury: a neurophysiological model of the bases of recovery from stroke. Prog Brain Res 1987;71:249–66.

Jezzard P, Matthews PM, Smith SM, editors. Functional magnetic resonance imaging: an introduction to methods. Oxford UK: Oxford University Press; 2001. p. 390.

Kastner S, Ungerleider LG. Mechanisms of visual attention in the human cortex. Annu Rev Neurosci 2000;23:315–41.

Kourtzi Z, Tolias AS, Altmann CF, Augath M, Logothetis NK. Integration of local features into global shapes: monkey and human FMRI studies. Neuron 2003;37(2):333–46.

Koyama M, Hasegawa I, Osada T, Adachi Y, Nakahara K, Miyashita Y. Functional magnetic resonance imaging of macaque monkeys performing visually guided saccade tasks; comparison of cortical eye fields with humans. Neuron 2004;41(5):795–807.

Leite FP, Tsao D, Vanduffel W, Fize D, Sasaki Y, Wald LL, et al. Repeated fMRI using iron oxide contrast agent in awake, behaving macaques at 3 T. Neuroimage 2002;16(2):283–94.

Leopold DA, Plettenberg HK, Logothetis NK. Visual processing in the ketamine-anesthetized monkey. Optokinetic and blood oxygenation level-dependent responses. Exp Brain Res 2002;143(3):359–72.

Logothetis NK, Guggenberger H, Peled S, Pauls J. Functional imaging of the monkey brain. Nat Neurosci 1999;2(6):555–62.

Logothetis NK, Pauls J, Augath M, Trinath T, Oeltermann A. Neurophysiological investigation of the basis of the fMRI signal. Nature 2001;412(6843):150–7.

Mao H, Kidambi S. Reduced susceptibility artifacts in BOLD fMRI using localized shimming. Neuroimage 2000;11(5):S553.

Matsuura H, Inoue T, Konno H, Sasaki M, Ogasawara K, Ogawa A. Quantification of susceptibility artifacts produced on high-field magnetic resonance images by various biomaterials used for neurosurgical implants. J Neurosurg 2002;97(6):1472–5 Technical note.

Moore T, Rodman HR, Gross CG. Direction of motion discrimination after early lesions of striate cortex (V1) of the macaque monkey. Proc Natl Acad Sci USA 2001;98(1):325–30.

Moore T, Rodman HR, Repp AB, Gross CG, Mezrich RS. Greater residual vision in monkeys after striate cortex damage in infancy. J Neurophysiol 1996;76(6):3928–33.

Nakahara K, Hayashi T, Konishi S, Miyashita Y. Functional MRI of macaque monkeys performing a cognitive set-shifting task. Science 2002;295(5559):1532–6.

Nakamura K, Chung HH, Graziano MS, Gross CG. Dynamic representation of eye position in the parieto-occipital sulcus. J Neurophysiol 1999;81(5):2374–85.

Orban GA, Fize D, Peuskens H, Denys K, Nelissen K, Sunaert S, et al. Similarities and differences in motion processing between the human and macaque brain: evidence from fMRI. Neuropsychologia 2003;41(13):1757–68.

Payne BR, Lomber SG. Reconstructing functional systems after lesions of cerebral cortex. Nat Rev Neurosci 2001;2(12):911–9.

Perrett DI, Rolls ET, Caan W. Visual neurones responsive to faces in the monkey temporal cortex. Exp Brain Res 1982;47(3):329–42.

Pinsk MA, Moore T, Richter M, Gross CG, Kastner S. Functional MRI in behaving monkeys. Soc Neurosci Abstr 2003;29(69):19.

Rainer G, Augath M, Trinath T, Logothetis NK. The effect of image scrambling on visual cortical BOLD activity in the anesthetized monkey. Neuroimage 2002;16(3 Pt 1):607–16.

Rainer G, Augath M, Trinath T, Logothetis NK. Nonmonotonic noise tuning of BOLD fMRI signal to natural images in the visual cortex of the anesthetized monkey. Curr Biol 2001;11(11):846–54.

Reese TG, Davis TL, Weisskoff RM. Automated shimming at 1.5 T using echo-planar image frequency maps. J Magn Reson Imaging 1995;5(6):739–45.

Rodman HR, Gross CG, Albright TD. Afferent basis of visual response properties in areaMT of the macaque. I. Effects of striate cortex removal. J Neurosci 1989;9(6):2033–50.

Schmitt F, Stehling MK, Turner R, Bandettini PA, editors. Echo-planar imaging: theory, technique and application. Berlin Germany: Springer-Verlag; 1998.

Sereno ME, Trinath T, Augath M, Logothetis NK. Three-dimensional shape representation in monkey cortex. Neuron 2002;33(4):635–52.

Sled JG, Zijdenbos AP, Evans AC. A nonparametric method for automatic correction of intensity nonuniformity in MRI data. IEEE Trans Med Imaging 1998;17(1):87–97.

Smith SM. Flexible filter neighborhood designation. Proc 13th Int Conf on Pattern Recognition 1996;1:206–12.

Smith SM. Fast robust automated brain extraction. Hum Brain Mapp 2002;17(3):143–55.

Stefanacci L, Reber P, Costanza J, Wong E, Buxton R, Zola S, et al. fMRI of monkey visual cortex. Neuron 1998;20(6):1051–7.

Teo PC, Sapiro G, Wandell BA. Creating connected representations of cortical gray matter for functional MRI visualization. IEEE Trans Med Imaging 1997;16(6):852–63.

Tolias AS, Smirnakis SM, Augath MA, Trinath T, Logothetis NK. Motion processing in the macaque: revisited with functional magnetic resonance imaging. J Neurosci 2001;21(21):8594–601.

Tsao DY, Freiwald WA, Knutsen TA, Mandeville JB, Tootell RB. Faces and objects in macaque cerebral cortex. Nat Neurosci 2003a;6(9):989–95.

Tsao DY, Vanduffel W, Sasaki Y, Fize D, Knutsen TA, Mandeville JB, et al. Stereopsis activates V3 A and caudal intraparietal areas in macaques and humans. Neuron 2003b;39(3):555–68.

Ungerleider LG, Desimone R. Cortical connections of visual area MT in the macaque. J Comp Neurol 1986;248(2):190–222.

Van Essen DC. Organization of visual areas in macaque and human cerebral cortex. In: The Visual Neurosciences. Cambridge MA: MIT Press; 2004 p. 507–21.

Van Essen DC. Windows on the brain: the emerging role of atlases and databases in neuroscience. Curr Opin Neurobiol 2002;12(5):574–9.

Van Essen DC, Drury HA, Dickson J, Harwell J, Hanlon D, Anderson CH. An integrated software suite for surface-based analyses of cerebral cortex. J Am Med Inform Assoc 2001;8(5):443–59.

Vanduffel W, Fize D, Mandeville JB, Nelissen K, Van Hecke P, Rosen BR, et al. Visual motion processing investigated using contrast agent-enhanced fMRI in awake behaving monkeys. Neuron 2001;32(4):565–77.

Vanduffel W, Fize D, Peuskens H, Denys K, Sunaert S, Todd JT, et al. Extracting 3D from motion: differences in human and monkey intraparietal cortex. Science 2002;298(5592):413–5.

Weyand TG, Malpeli JG. Responses of neurons in primary visual cortex are modulated by eye position. J Neurophysiol 1993;69(6):2258–60.

Xerri C, Merzenich MM, Peterson BE, Jenkins W. Plasticity of primary somatosensory cortex paralleling sensorimotor skill recovery from stroke in adult monkeys. J Neurophysiol 1998;79(4):2119–48.

Young IR, Cox IJ, Bryant DJ, Bydder GM. The benefits of increasing spatial resolution as a means of reducing artifacts due to field inhomogeneities. Magn Reson Imaging 1988;6(5):585–90.